

Investigations of a two-mode atom laser model

Jens Schneider* and Axel Schenzle†

*Max-Planck-Institut für Quantenoptik, Hans-Kopfermann-Straße 1, D-85748 Garching and
Sektion Physik, Ludwig-Maximilians-Universität München, Theresienstraße 37, D-80333 München, Germany*
(submitted to Phys. Rev. A, October 27, 1999)

Atom lasers based on rf-outcoupling from a trapped Bose-Einstein condensate can be described by a set of generalized, coupled Gross-Pitaevskii equations (GPE).

If not only one but two radio frequencies are used for outcoupling, the atoms emerging from the trap have two different energies and the total wavefunction of the untrapped spin-state is a coherent superposition which leads to a pulsed atomic beam.

We present results for such a situation obtained from a 1D-GPE model for magnetically trapped Rb-87 in the $F = 1$ state. The wavefunction of the atomic beam can be approximated by a sum of two Airy functions. In the limit of weak coupling we calculate the intensity analytically.

03.75.-Fi,05.30.Jp

I. INTRODUCTION

Now, as the creation of trapped Bose-Einstein condensates [1–3] has nearly become a standard technique, the interest in the field has turned to the manipulation of trapped condensates. A major goal is the creation of coherent atomic beams emerging from Bose condensates. Such a device, now called an atom laser, was first realized in the MIT-group [4]. This experiment created a rather small number of strong pulses of atoms. Recently two groups were able to produce continuous [5] or at least quasi-continuous [6] coherent atomic beams.

After the initial proposals of atom-laser models (see references in [7]) the theoretical treatment of atom lasers has focused on two major lines: the work in [8–19] starts with the coupled Gross-Pitaevskii equations (GPE) (and generalizations thereof like the Hartree-Fock-Bogoliubov theory) and analyzes the corresponding solutions either numerically or analytically.

On the other hand, the studies in [20–25] concentrate on the characterization of atom lasers using master equations analogous to the work on optical lasers and calculate properties like the linewidth of atom lasers.

There are two different means of coherent outcoupling, *i.e.* getting atoms out of atom traps, which are investigated both theoretically and experimentally. A radio

frequency can be used to flip the spin-state of magnetically trapped atoms to an untrapped state; this so called radio-frequency outcoupling [8] has been used in [4,5]. An output coupler based on Raman transitions was first described in [26] and implemented by the NIST-group [6]. In rf-outcoupling, the atomic beam just falls downwards whereas two-photon Raman-outcoupling can be arranged in such a way that the outcoupled atoms acquire momentum and the resulting beam may thus be pointed in a specific direction.

Like in our previous work [19] we concentrate on rf-outcoupling describing the setup of the Hänsch-group [5] by a 1D-model based on coupled GPEs. In [19] we were able to characterize the experimental output rate in a satisfactory way, differences were mainly due to the reduced dimensionality of the model. Here, we want to investigate a slightly different setup that was recently realized experimentally: instead of only one rf-field Bloch *et al.* [27] used two radio frequencies for outcoupling. Consequently, the coherently outcoupled atoms have two different energies which leads to a pulsed, coherent atomic beam. We will analyze the output properties of such a device depending on the detunings of the radio frequencies and their difference.

The paper has the following structure: In Sec. II we set the notation by introducing the basic facts about GPEs and rf-atom lasers. In Sec. III we first show how stationary falling waves can be described by appropriate combinations of Airy functions. These are used to model the output of the two-mode atom laser and to calculate its average output rate. The analytical results of this section are then compared with numerical solutions of the coupled GPEs (Sec. IV). It turns out that the visibility of the pulse pattern of the beam can be related to the correlation function of the trapped Bose gas (here at $T = 0$, see also [27]). In Sec. V we summarize our results.

II. COUPLED GROSS-PITAEVSKII EQUATIONS WITH TWO RADIO FREQUENCIES

The properties of Bose condensates of atomic vapors at zero temperature are very well described by the Gross-Pitaevskii equation (GPE) (see [28] and references therein). It is a nonlinear Schrödinger equation for the order parameter of the system, namely the macroscopic wavefunction of the Bose condensate, and accounts also for the coherence properties of the condensate. It may thus serve as a starting point for considerations in coher-

*E-mail: jens.schneider@mpq.mpg.de

†E-mail: axel.schenzle@physik.uni-muenchen.de

ent atom optics with Bose condensates as it was done in [8]: the authors generalized the GPE to a system of coupled equations that describe the physics of the trapped and untrapped states of a Bose gas coupled via an rf-field including the interaction due to collisions.

In the present article, we modify this approach to a situation where the trapped atoms are exposed to two radio frequencies. Such a setup has already been analyzed experimentally [27]. We focus on a trap with Rb-87 atoms in the $F = 1$ hyperfine-manifold. The three Zeeman sub-levels with $m \in \{-1, 0, 1\}$ are described by macroscopic wavefunctions ψ_m ; after applying the dipole approximation the system of generalized GPEs reads

$$i\hbar \frac{\partial}{\partial t} \psi_m(\vec{r}, t) = \left(-\frac{\hbar^2 \nabla^2}{2M} + V_m(\vec{r}) + U |\psi(\vec{r}, t)|^2 \right) \psi_m(\vec{r}, t) + \sum_{m'} W_{m,m'} \psi_{m'}(\vec{r}, t). \quad (1)$$

We assume that all Zeeman levels interact with the same s-wave scattering length $a_0 = 110 a_{\text{Bohr}}$ so $U = 4\pi\hbar^2 a_0 N/M$. $|\psi(\vec{r}, t)|^2 = \sum_m |\psi_m(\vec{r}, t)|^2$ denotes the total density in the trap divided by the number N of particles. The interaction between the atoms and the radio frequency fields with frequencies $\omega_{\text{rf},1}$ and $\omega_{\text{rf},2}$ is described by

$$W_{m,m'} = 2\hbar\Omega (\cos(\omega_{\text{rf},1}t) + \cos(\omega_{\text{rf},2}t)) \times (\delta_{m,m'+1} + \delta_{m,m'-1}), \quad (2)$$

where $\Omega = g_F \mu_{\text{Bohr}} B_{\text{rf}} / (\sqrt{2}\hbar)$ ($g_F = 1/2$) is the Rabi frequency corresponding to the magnetic field strength B_{rf} .

We now define $\bar{\omega}_{\text{rf}} = (\omega_{\text{rf},1} + \omega_{\text{rf},2})/2$ to be the average radio frequency and $\delta_{\text{rf}} = \omega_{\text{rf},1} - \omega_{\text{rf},2}$ as the difference between the two driving fields. In order to get rid of the high frequencies, we apply the transformation $\psi_m(t) \rightarrow e^{-im\bar{\omega}_{\text{rf}}t} \psi_m(t)$ and skip all terms $\propto \exp(-2im\bar{\omega}_{\text{rf}}t)$ (rotating wave approximation). This turns Eq. (1) into

$$i\hbar \frac{\partial}{\partial t} \psi_m(\vec{r}, t) = \left(-\frac{\hbar^2 \nabla^2}{2M} + V_m(\vec{r}) + m\hbar\bar{\omega}_{\text{rf}} + U |\psi(\vec{r}, t)|^2 \right) \psi_m(\vec{r}, t) + \sum_{m'} \tilde{W}_{m,m'}(t) \psi_{m'}(\vec{r}, t) \quad (3)$$

with

$$\tilde{W}_{m,m'}(t) = 2\hbar\Omega \cos(\delta_{\text{rf}}t/2) (\delta_{m,m'+1} + \delta_{m,m'-1}). \quad (4)$$

Equation (3) represents a set of equations in three dimensions that has to be solved numerically. This is computationally very demanding. In earlier work [8,11,12,19]

a one-dimensional (1D) approach has proven to be quite successful. Usually, the traps used in experiments are elongated in the horizontal plane. Like in [19] we choose coordinates where the z -axis points *downwards*, the long axis of the trap is denoted by y , the short horizontal one by x . Taking gravity into account, the total effective potentials in z -direction are then given by

$$V_{m,\text{eff}}(z, t) = -mM\omega_z^2 z^2 / 2 + m\hbar\Delta - Mgz + g_{1\text{D}} |\psi(z, t)|^2, \quad (5)$$

where $\Delta = \hbar\bar{\omega}_{\text{rf}} - V_{\text{off}}$ denotes the detuning from the transitions at the trap center ($V_{\text{off}} = -g_F \mu_{\text{Bohr}} B_{\text{off}}$). Due to gravity the output coupling proceeds mainly in the vertical direction so it is natural to choose this direction as the 1D axis for our model.

To obtain the effective interaction strength $g_{1\text{D}}$ in Eq. (5) we require the chemical potential in Thomas-Fermi approximation in the 1D model (for the trapped $m = -1$ state) to equal the one of the full 3D situation. This leads to

$$g_{1\text{D}} = \frac{2}{3} \left(\frac{\omega_y}{\omega_z} \right)^{\frac{3}{5}} \left(\frac{15Na_0}{a_z} \right)^{\frac{3}{5}} \hbar\omega_z a_z \quad (6)$$

with $a_z = \sqrt{\hbar/(M\omega_z)}$.

The 1D approximation of Eq. (3) then reads

$$i\hbar \frac{\partial}{\partial t} \psi_m(z, t) = \left(-\frac{\hbar^2}{2M} \frac{\partial^2}{\partial z^2} + V_{m,\text{eff}}(z, t) \right) \psi_m(z, t) + \sum_{m'} \tilde{W}_{m,m'}(t) \psi_{m'}(z, t). \quad (7)$$

In this work, we concentrate on the weak coupling regime of Eq. (7) which is characterized by $\Omega < \omega_z$ [4,12,17]. The condensate is hardly affected in this regime, it merely changes its overall size due to the loss of atoms by the outcoupling process [12]. In [19] we have pointed out that the coupling between the trapped and untrapped states is concentrated spatially to the crossing points of the effective potentials in Eq. (5). In the present case where two radio frequencies are present, one expects two such points of maximal coupling. They are located at

$$z_{\text{rf},1,2} = \sqrt{2(\Delta \pm \delta_{\text{rf}}/2)/(\hbar\omega_z)} a_z, \quad (8)$$

corresponding again to the crossing points of the effective potentials for either the radio frequency $\omega_{\text{rf},1}$ or $\omega_{\text{rf},2}$ (see Fig. 2). In Fig. 1 the densities of the states $m = -1$ and 0 ($F = 1$) are shown for a specific situation. The condensate is in the $m = -1$ state, the plot shows a snapshot of the density distributions after 5 ms of outcoupling (for further computational details see Sec. IV). The distribution for the $m = 0$ state demonstrates clearly that the points $z_{\text{rf},1,2}$ are indeed the points of maximum outcoupling; if one considers the two radio frequencies separately, these points correspond to the classical turning points in the effective potentials in Eq. (5) (see [19]).

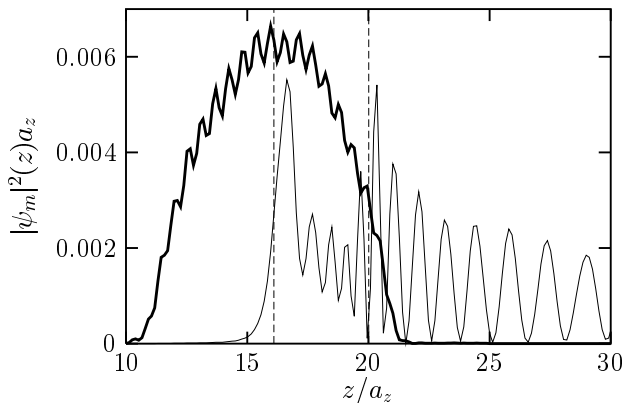


FIG. 1. Plot of the densities for $m = -1, 0$ ($F = 1$) in the trap for weak outcoupling. The trapped $m = -1$ state (thick line, scaled down by a factor of 20) shows some small excitations on top of the ground state. The untrapped $m = 0$ state (thin line) exhibits pulses for $z \gtrsim 23 a_z$. The dashed lines denote the resonance points $z_{\text{rf},1,2}$ from Eq. (8), here we have $\omega_{\text{rf},1,2} = 2\pi \times (21000 \pm 4500)$ Hz.

In the weak coupling region we are considering here, the state $m = 1$, which is also untrapped, is hardly populated at all. For this reason, its density distribution is not shown in Fig. 1 and we will not discuss it further. Nevertheless, it is included in all numerical calculations.

III. AIRY FUNCTIONS FOR FALLING ATOMS AND OUTPUT FLUX

A. Stationary, falling waves

Outside the condensate region, the untrapped $m = 0$ state feels only the gravitational potential because the mean field contribution in $V_{0,\text{eff}}$ is practically zero there. Therefore, the wavefunction for the falling particles is a linear combination of Airy functions, which are the solutions of the Schrödinger equation for a linear potential. The usual Airy function $\text{Ai}(\xi)$ does not suffice to describe a continuous, stationary beam of falling atoms. In analogy to free planar waves, where both cosine and sine are used to form a traveling wave $\propto \exp(ikx)$, we have to use a special complex solution of the Schrödinger equation for a given energy E

$$\begin{aligned} \psi_E(z, t) &= \{ \text{Ai}(-\xi_E(z)) - i \text{Bi}(-\xi_E(z)) \} e^{-iEt/\hbar} \\ &= \mathcal{M}(\xi_E(z)) e^{-i[\Theta(\xi_E(z)) + Et/\hbar]} . \end{aligned} \quad (9)$$

The argument $\xi_E(z)$ simply shifts and rescales the z -axis

$$\xi_E(z) = \frac{1}{l} \left(z + \frac{E}{Mg} \right), \quad l = \left(\frac{\hbar^2}{2M^2g} \right)^{1/3}, \quad (10)$$

where l is a length scale (see e.g. [29]). The wavefunction $\psi_E(z, t)$, though being a solution of the Schrödinger

equation for a homogenous gravitational field, is not normalizable due to the exponential growth of $\text{Bi}(\xi_E(z))$ in the classical forbidden region $z < -E/(Mg)$. This is to be expected, as it describes a situation where particles are flowing steadily to $z \rightarrow \infty$ without a source of particles at some finite z . Nevertheless, we are only interested in the classically allowed region where the solution is perfectly analogous to a freely falling wave.

We will later make use of the asymptotic forms ($z \rightarrow \infty$) of $\mathcal{M}(\xi)$ and $\Theta(\xi)$ [30]

$$\begin{aligned} \mathcal{M}(\xi) &\approx \frac{1}{\sqrt{\pi}} \xi^{-1/4} \\ \Theta(\xi) &\approx \frac{\pi}{4} - \frac{2}{3} \xi^{3/2} \end{aligned} \quad (11)$$

to obtain a nice interpretation for $|\psi_0(z, t)|^2$.

B. Coherent superposition of two falling waves

The two radio frequencies driving the condensate should lead to two different energies in the resulting atomic beam (see Fig. 2).

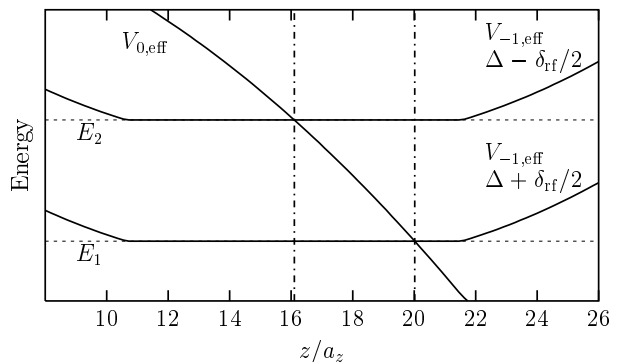


FIG. 2. Effective potentials $V_{m,\text{eff}}$ and energies $E_{1,2}$ of the outcoupled atoms for the two detunings $\Delta \pm \delta_{\text{rf}}/2$. The two vertical lines denote the resonance points $z_{\text{rf},1,2}$.

The energy of the outcoupled beam for a detuning Δ is given by

$$E = \mu - \frac{1}{2} \frac{Mg^2}{\omega_z^2} - \hbar\Delta, \quad (12)$$

where μ denotes the chemical potential. If we consider the radio frequencies $\omega_{\text{rf},1}$ and $\omega_{\text{rf},2}$, we have to use the two detunings $\Delta_{1,2} = \hbar\omega_{\text{rf},1,2} - V_{\text{off}}$ to get the energies $E_{1,2}$ indicated in Fig. 2.

Assuming that the outcoupling process proceeds in a fully coherent way, the total wavefunction of the outcoupled beam is given by

$$\psi_0(z, t) = \mathcal{N}(\psi_{E_1}(z, t) + s\psi_{E_2}(z, t)), \quad (13)$$

where \mathcal{N} is an overall normalization constant and s accounts for the relative strength of the two contributing waves. In experiment, one usually measures the probability density $|\psi_0(z, t)|^2$ via some imaging technique. If the two energies $E_{1,2}$ are not too different from each other with respect to the mean energy $\bar{E} = (E_1 + E_2)/2$, *i.e.* $\hbar\delta_{\text{rf}}/\bar{E} \ll 1$, then Eq. (13) can be Taylor-expanded around \bar{E} . Taking the asymptotic forms in Eq. (11) into account, we can write $|\psi_0(z, t)|^2$ as

$$|\psi_0(z, t)|^2 = \tilde{\mathcal{N}}^2 \mathcal{M}^2(\xi_{\bar{E}}(z)) \times \{2 + 2P \cos(\phi(z, t) - \alpha)\} \quad (14)$$

with the phase

$$\phi(z, t) = \delta_{\text{rf}}t - \frac{\hbar\delta_{\text{rf}}}{Mgl} \sqrt{\xi_{\bar{E}}(z)}, \quad (15)$$

the modified norm

$$\tilde{\mathcal{N}}^2 = \mathcal{N}^2 \frac{1 + |s|^2}{2}, \quad (16)$$

and

$$P = \frac{2|s|}{1 + |s|^2}. \quad (17)$$

Apart from the \mathcal{M}^2 -dependence, Eq. (14) has the typical form of an interference term with P being the visibility. The maxima of this term describe the falling of pulses emerging from the trap. They are located at

$$z_k = -\frac{\bar{E}}{Mg} + \frac{1}{2}g \left(t - \frac{2\pi k + \alpha}{\delta_{\text{rf}}} \right)^2, \quad k \in \mathbb{N}_0, \quad (18)$$

corresponding to a pulse frequency $\nu_{\text{pulse}} = \delta_{\text{rf}}/(2\pi)$. This is exactly in analogy to “mode-locking” of two modes in a laser.

The phase α of $s = |s|e^\alpha$ appearing in the above equations is responsible for a shift of the interference pattern *i.e.* the pulses. Eq. (13) describes the output of the atom laser only after it has reached a kind of stationary operation. We therefore use α merely as a free parameter to shift the pulses in time.

C. Rate of outcoupling

To determine the normalization factor of the wavefunction \mathcal{N} in Eq. (13) we use the fact that in 1D the flux density j_z equals directly the rate of atoms going through a point. j_z can be written as

$$j_z(z, t) = |\psi_0(z, t)|^2 v_z(z), \quad (19)$$

$$v_z(z) = -\frac{\hbar}{M} \frac{\partial \Theta}{\partial z} = \frac{\hbar}{Ml} \sqrt{\xi_{\bar{E}}(z)}, \quad (20)$$

v_z being the velocity of atoms in z-direction. Eq. (20) is obtained by considering only the leading terms in $\xi_E(z)$

for $z \rightarrow \infty$. Averaging over time in Eq. (19) finally leads to

$$j_z = \frac{\hbar}{2\pi Ml} \tilde{\mathcal{N}}^2. \quad (21)$$

In [12], Steck *et al.* gave a formula for the outcoupling rate of a three dimensional trap in the weak coupling limit. Analogously, this result can be derived for the 1D situation we are interested in (see [31]). The rate for one resonance point z_{res} (resulting from a detuning Δ) is given by

$$\Gamma_{z_{\text{res}}}^{\text{1d}} = 2\pi \left(\frac{\Omega}{\omega_z} \right)^2 \frac{|\psi_{-1}(z_{\text{res}})|^2}{\sqrt{2\Delta/\omega_z}} a_z \omega_z. \quad (22)$$

We now assume that the rates at the two resonance points $z_{\text{rf},1,2}$ add up to the total outcoupling rate. This rate must be equal to j_z , so finally with the help of Eq. (21) we arrive at an expression for the normalization

$$\tilde{\mathcal{N}}^2 = \frac{\pi Ml}{2\hbar} \left(\Gamma_{z_{\text{rf},1}}^{\text{1d}} + \Gamma_{z_{\text{rf},2}}^{\text{1d}} \right), \quad (23)$$

where $\Gamma_{z_{\text{rf},1,2}}^{\text{1d}}$ is obtained from the detunings $\Delta \pm \delta_{\text{rf}}/2$.

Inspection of Eq. (13) shows that $|s|$ should reflect the relative outcoupling rates at the two resonance points. We define it via

$$|s|^2 = \frac{\Gamma_{z_{\text{rf},1}}^{\text{1d}}}{\Gamma_{z_{\text{rf},2}}^{\text{1d}}}, \quad (24)$$

which leads to

$$P = 2 \frac{\sqrt{\Gamma_{z_{\text{rf},1}}^{\text{1d}} \Gamma_{z_{\text{rf},2}}^{\text{1d}}}}{\Gamma_{z_{\text{rf},1}}^{\text{1d}} + \Gamma_{z_{\text{rf},2}}^{\text{1d}}} \quad (25)$$

for the visibility. The numerical results in the next section show that this is indeed the correct expression. If the frequency difference δ_{rf} is very small, one can also use

$$\tilde{\mathcal{N}}^2 = \frac{\pi Ml}{\hbar} \Gamma_{z_{\text{res}}}^{\text{1d}}, \quad (26)$$

$$|s|^2 = \frac{|\psi_{-1}(z_{\text{rf},1})|^2}{|\psi_{-1}(z_{\text{rf},2})|^2}, \quad (27)$$

$$P = 2 \frac{|\psi_{-1}(z_{\text{rf},1})| |\psi_{-1}(z_{\text{rf},2})|}{|\psi_{-1}(z_{\text{rf},1})| + |\psi_{-1}(z_{\text{rf},2})|}, \quad (28)$$

which shows that P is related to the correlation function of the trapped Bose gas [27].

IV. NUMERICAL RESULTS

A. Numerical method and observation of pulses

To solve the 1D GPEs in Eq. (7) numerically we propagate the wavefunctions with a usual split-operator algorithm using FFT on a 1D grid. As starting condition

we always use the ground state of the trapped $m = -1$ state, which we obtain by imaginary time propagation.

The coupling of the Zeeman levels via the rf-field is implemented in a very straightforward way: if the right hand side of Eq. (7) is written as $H\psi$, one can split up the Hamiltonian H in an obvious way $H = T + V(t) + W(t)$. The kinetic and potential parts T and $V(t)$ are taken care of by the FFT-split-operator technique. It is sufficient to treat the coupling part $W(t)$ separately in the most simple way by keeping only the terms up to first order in the propagation time. The propagator from time t to $t + \Delta t$ then reads

$$U(t, t + \Delta t) = U_0(t, t + \Delta t) \left(1 - \frac{i}{\hbar} W(t) \Delta t \right), \quad (29)$$

where U_0 is the split-operator propagator for $T + V(t)$.

The trap parameters are basically taken from [5], the trapping frequency for the $m = 1$ state is $\omega_z = 2\pi \times 127$ Hz. We often use harmonic oscillator units, the length unit is $a_z = 0.95 \mu\text{m}$, time is measured in $1/\omega_z = 1.3$ ms.

To investigate the output in our atom-laser model we have propagated the initial wavefunction for up to ≈ 30 ms with different coupling parameters. We kept the coupling strength rather low to ensure a clear separation of the time scales for Rabi oscillations and for the pulses predicted in the previous section. We typically use a magnetic field strength of $B_{\text{rf}} = 0.1$ mG that is also used in the latest experiments in the Hänsch group [27]. This amounts to a Rabi frequency of $\Omega = 2\pi \times 70$ Hz, which is less than the trapping frequency ω_z and the pulse frequency δ_{rf} (see below Eq. (18)). All calculations were done with $N = 5 \times 10^5$ atoms in the trap.

In Fig. (3) we show the density distribution of the outcoupled state as a function of both space and time. The atomic beam emerging from the condensate clearly exhibits the pulses predicted in section III B.

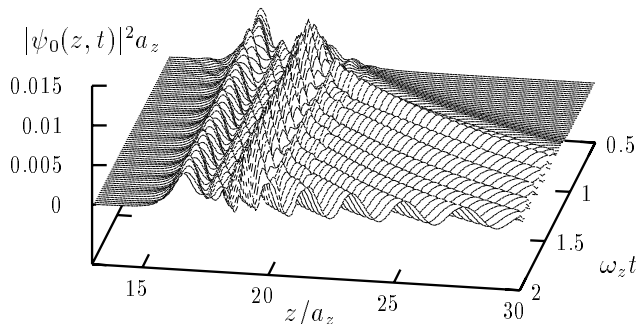


FIG. 3. Plot of the outcoupled density. The atoms in the free $m = 0$ state emerge primarily at the two resonance points (cf. Fig. 1) and then fall downwards (to the right in the plot). One can clearly see the pulse trains emerging from the condensate region that extends to $z \approx 22 a_z$. The radio frequency detunings in this plot are $\Delta_{1,2} = 2\pi \times (19.5 \pm 3.0)$ kHz.

To prove that these pulses really follow the trajectories in Eq. (18), Fig. 4 shows a contour plot of the data in Fig. 3. As we mentioned in Sec. III B, we used the phase α in Eq. (18) to shift the trajectories in time. Apart from this, the pulses show the correct behavior, they start between the two resonance points at $-\bar{E}/(Mg)$ and appear with the right frequency.

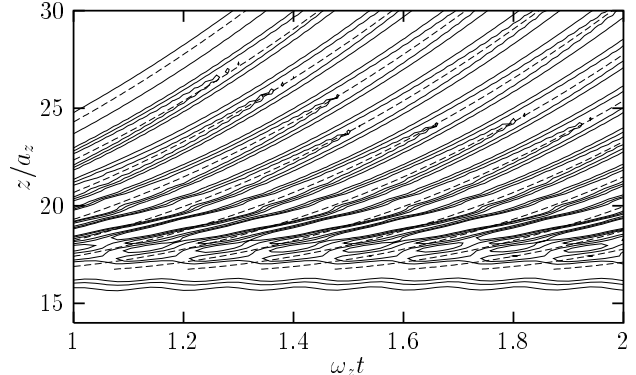


FIG. 4. Contour plot of the data in Fig. 3. The full lines are the contour lines for $|\psi_0(z, t)|^2 a_z = 0.001, 0.002, 0.003$. The dashed lines denote the trajectories of the pulse maxima from Eq. (18).

B. Output rates and visibility

In this section we want to compare the numerical results to the analytic predictions of Sec. III. All results were obtained by keeping the frequency $\omega_{\text{rf},2}$ fixed such that the corresponding resonance point is at the center of the condensate ($z_{\text{rf},2} = z_{\text{sag}} = g/\omega_z^2$, $\Delta_2 = 2\pi \times 16.5$ kHz). Δ_1 is then given by $\Delta_1 = \Delta_2 + \delta_{\text{rf}}$; we consider only positive rf differences $\delta_{\text{rf}} = 0 \dots 2\pi \times 13$ kHz.

The visibility in Fig. 1 is rather high, namely $P = 0.90$. If one increases δ_{rf} , the visibility drops down, as can be seen in Fig. 5. This is due to the fact that it depends mainly on the quotient of the wavefunctions at the resonance points (see Eqs. (24,25,22)), which decreases if one pushes $z_{\text{rf},1}$ further to the boundary of the condensate.

One can now take Eqs. (22,25,14) to calculate the visibility and the norm of the Airy functions from Sec. III using the values of $|\psi_{-1}(z_{\text{rf},1,2})|$ either from the Thomas-Fermi (TF) approximation [28] or directly from the numerical calculations. The dashed line in Fig. 5 is obtained in this way using the numerical values, outside the condensate it fits the numerical calculations quite well. The Thomas-Fermi result (not shown) is only slightly different. The total output rate $\Gamma_{z_{\text{rf},1}}^{1d} + \Gamma_{z_{\text{rf},2}}^{1d}$ can be calculated via Eq. (23) from \tilde{N}^2 ; we compared it to the initial decay constant of the condensate occupation and found good agreement.

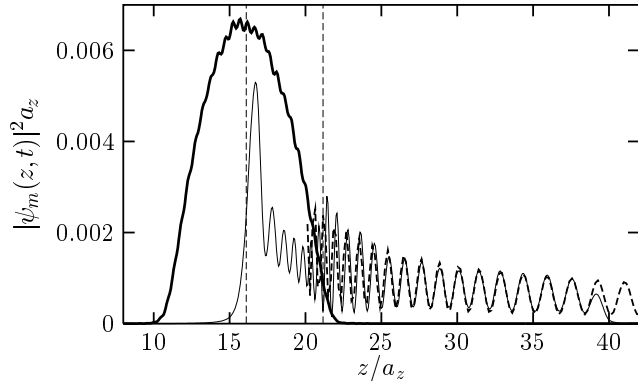


FIG. 5. Plot of the density distributions of the atom laser (see also Fig. 1). This plot is made after 5 ms of operation with $\delta_{\text{rf}} = 2\pi \times 12000$ Hz. The right resonance point is in the wing of the condensate so the visibility drops to $P = 0.61$. The dashed line is a plot of the function in Eq. (14) with the normalization of Eq. (23). The density of the untrapped state goes down to zero around $z = 40 a_z$ due to absorbing boundary conditions used in the calculations.

After having shown that the output can be characterized by the wavefunction in Eq. (14), we want to compare further the semi-analytic results of Sec. III to the numerics. For different δ_{rf} one can plot the visibilities obtained either by fitting the data or by calculating P via (25) using the TF-approximation or the values of $|\psi_{-1}(z_{\text{rf},1,2})|$ from the numerics. Fig. 6 demonstrates the result: the TF-approximation (full line) fits the semi-analytic values (triangles) quite well. Like in an experiment, we tried to fit the density distribution (14) to our numerical data at a fixed time to get values for P . As the figure shows, these values are in a reasonable agreement with the other results.

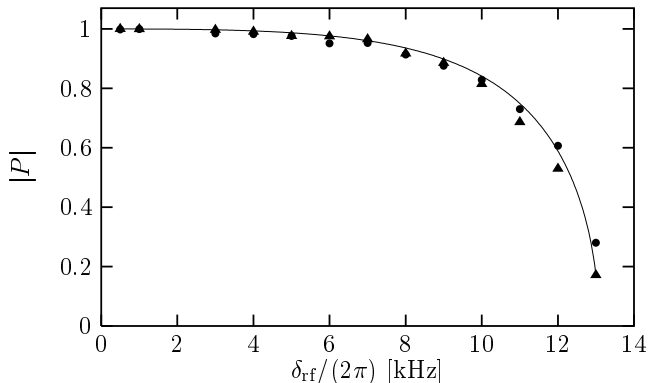


FIG. 6. Visibility versus radio frequency difference. The full line is obtained from the Thomas-Fermi approximation. The triangles are calculated from the numerical values of $|\psi_{-1}(z_{\text{rf},1,2})|$ at a specific time. The points denoted by circles are obtained by fitting the density distribution (14) to the numerical data at fixed time (after ≈ 7.5 ms of outcoupling). The error for these values is smaller than 5% and was conservatively deduced from the fitting procedure.

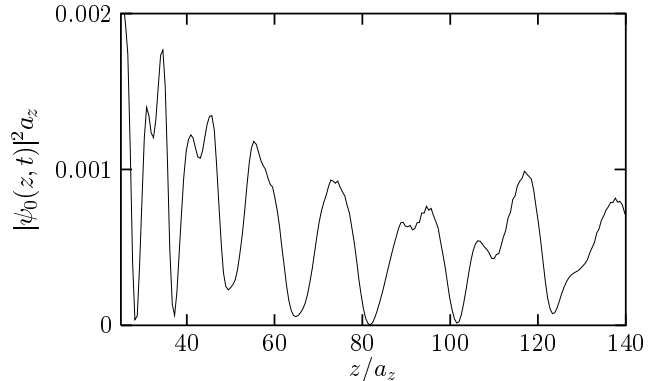


FIG. 7. Density distribution of the untrapped state for $\delta_{\text{rf}} = 2\pi \times 2000$ Hz. The pulses have a substructure originating from roughly twice the difference frequency δ_{rf} .

In Fig. 6 we have not shown values for $\delta_{\text{rf}} = 2\pi \times 2$ kHz. The reason for this is a resonance phenomenon in this region that leads to a more complicated pulse structure (Fig. 7) and prevents us from fitting (14) to the data. The origin of this resonance is unclear up to now, there are indications however that it is related to the creation of small particle-like excitations in the condensate via a process that is second order in the output coupling strength.

The small wiggles on top of the condensate density distribution in Figs. 1 and 5 indicate the presence of such excitations also for δ_{rf} away from $2\pi \times 2$ kHz. They are so small for these frequency differences that the assumption made above Eq. (23) that the outcoupling process proceeds as if the two radio frequencies were applied separately is really satisfied, *i.e.* there are hardly any processes of second order in the rf-coupling $\hbar\Omega$.

V. CONCLUSION

We have shown in this work that a rf-atom laser driven by two radio frequencies — a two-mode atom laser — gives rise to a coherently pulsing beam of atoms. We have given formulas for the output rate of such a device and for the visibility of the pulse pattern of the atomic beam. These analytic results are valid for atom lasers operated at very low temperature (virtually $T = 0$) and with weak output coupling.

The main limitation of our results comes from dimensionality: we use a 1D model for our calculations instead of a full 3D treatment. In [19] we have shown that the output rate of a rf-atom laser operated with one frequency can be calculated by the 1D model in qualitative agreement with experiment. Accordingly, apart from quantitative agreement of the output rates our model reproduces the experimental features quite well [27].

We did not address the problem of a pump for a true cw-atom laser. Instead, we considered rather small couplings that ensure a continuous and smooth operation for

about 20–50 ms but with slowly decreasing output rates. After this time only very few atoms are left in the atom trap. The output of a true cw-atom laser should be very similar to that of our situation.

Coherently pulsing beams of atoms are certainly of interest for applications in quantum and atom optics. The setup described in this paper produces beams that always point downwards due to gravity. It should be possible to use a similar setup with two different two-photon Raman transitions to create a pulsed beam that can be pointed in any direction by using the momentum kick from the absorption-emission process.

Finally, if one uses more than two frequencies, one might create pulsed beams with shorter pulses while keeping their repetition rate fixed in analogy to a mode-locked optical laser [32].

ACKNOWLEDGMENTS

We thank Immanuel Bloch and Tilman Esslinger for fruitful discussions. Financial support by DFG under Grant Nr. SCHE 128/7-1 is gratefully acknowledged.

- [21] G. M. Moy, J. J. Hope, and C. M. Savage, *Phys. Rev. A* **59**, 667 (1999).
- [22] M. W. Jack, M. Naraschewski, M. J. Collett, and D. F. Walls, *Phys. Rev. A* **59**, 2962 (1999).
- [23] J. Hope, G. M. Moy, M. J. Collett, and C. M. Savage, (1999), cond-mat/9901073.
- [24] J. Hope, G. M. Moy, M. J. Collett, and C. M. Savage, (1999), cond-mat/9907023.
- [25] H. P. Breuer, D. Faller, B. Kappler, and F. Petruccione, *Phys. Rev. A* **60**, 3188 (1999).
- [26] G. M. Moy, J. J. Hope, and C. M. Savage, *Phys. Rev. A* **55**, 3631 (1997).
- [27] I. Bloch, T. W. Hänsch, and T. Esslinger, to be published.
- [28] F. Dalfovo, S. Giorgini, L. P. Pitaevskii, and S. Stringari, *Rev. Mod. Phys.* **71**, 463 (1999).
- [29] S. Flügge, *Practical Quantum Mechanics* (Springer, Berlin, 1974).
- [30] *Handbook of Mathematical Functions*, edited by M. Abramowitz and I. A. Stegun (National Bureau of Standards, Washington, 1964), chapter 10.4.
- [31] H. Steck, Diplomarbeit, Universität München, 1997.
- [32] B. P. Anderson, and M. A. Kasevich, *Science* **282**, 1686 (1998).

-
- [1] M. H. Anderson *et al.*, *Science* **269**, 198 (1995).
 - [2] C. C. Bradley, C. A. Sackett, J. J. Tollett, and R. G. Hulet, *Phys. Rev. Lett.* **75**, 1687 (1995).
 - [3] K. B. Davis *et al.*, *Phys. Rev. Lett.* **75**, 3969 (1995).
 - [4] M.-O. Mewes *et al.*, *Phys. Rev. Lett.* **78**, 582 (1997).
 - [5] I. Bloch, T. W. Hänsch, and T. Esslinger, *Phys. Rev. Lett.* **82**, 3008 (1999).
 - [6] W. W. Hagley *et al.*, *Science* **283**, 1706 (1999).
 - [7] A. S. Parkins and D. F. Walls, prep **303**, 1 (1998).
 - [8] R. J. Ballagh, K. Burnett, and T. F. Scott, *Phys. Rev. Lett.* **78**, 1607 (1997).
 - [9] W. Zhang and D. F. Walls, *Phys. Rev. A* **57**, 1248 (1998).
 - [10] W. Zhang and D. F. Walls, *Phys. Rev. A* **58**, 4248 (1998).
 - [11] M. Naraschewski, A. Schenzle, and H. Wallis, *Phys. Rev. A* **56**, 603 (1997).
 - [12] H. Steck, M. Naraschewski, and H. Wallis, *Phys. Rev. Lett.* **80**, 1 (1998).
 - [13] B. Kneer *et al.*, *Phys. Rev. A* **58**, 4841 (1998).
 - [14] D. A. W. Hutchinson, *Phys. Rev. Lett.* **82**, 6 (1999).
 - [15] Y. Japha, S. Choi, K. Burnett, and Y. B. Band, *Phys. Rev. Lett.* **82**, 1079 (1999).
 - [16] R. Graham and D. F. Walls, *Phys. Rev. A* **60**, 1429 (1999).
 - [17] Y. B. Band, P. S. Julienne, and M. Trippenbach, *Phys. Rev. A* **59**, 3823 (1999).
 - [18] M. Edwards *et al.*, *J. Phys. B: At. Mol. Opt. Phys.* **32**, 2935 (1999).
 - [19] J. Schneider and A. Schenzle, *Appl. Phys. B* (1999), accepted.
 - [20] J. J. Hope, *Phys. Rev. A* **55**, R2531 (1997).